PHILOSOPHICAL TRANSACTIONS OF THE ROYAL SOCIETY A MATHEMATICAL, PHYSICAL & ENGINEERING SCIENCES

Compliant shell mechanisms

K. A. Seffen

Phil. Trans. R. Soc. A 2012 **370**, doi: 10.1098/rsta.2011.0347, published 19 March 2012

PHILOSOPHICAL TRANSACTIONS OF THE ROYAL SOCIETY A

Phil. Trans. R. Soc. A (2012) **370**, 2010–2026
doi:10.1098/rsta.2011.0347

Compliant shell mechanisms

By K. A. Seffen*

Department of Engineering, University of Cambridge, Trumpington Street, Cambridge CB2 1PZ, UK

This paper describes a class of lightweight structures known as compliant shell mechanisms. These are novel reconfigurable solutions for advanced structures, such as morphing shells and deployable membranes. They have local, discrete corrugations, which articulate and deform to achieve dramatic changes in the overall shape of the shell. The unique kinematics are considered by highlighting examples and by performing analysis using established and novel concepts, and favourable predictions of shape compared with laboratory models are demonstrated.

Keywords: compliant shell mechanisms; kinematical analysis; lightweight structures

1. Introduction

Compliant shell mechanisms are open, thin-walled, discretely corrugated structures, with flat facets or curved regions of shell interconnected by folds or hinge lines. The 'egg-box' in figure 1 [1] typifies their unusual properties: they are soft in certain directions before stiffening considerably, there is sometimes kinematical coupling between modes, they can be much stiffer in other directions from the outset, and they can be simply made—here, they are constructed from paper card. Their simplicity of form coupled to their unconventional performance may inspire novel solutions for advanced shell structures, for example, in so-called shape-changing (or 'morphing') aircraft [2], where traditional lightweight materials such as fibrous composites may falter. Developments in packaging may also benefit in structural and compaction terms, so that material usage and, ultimately, waste volume can be minimized.

Their compliance follows from the elastic deformation of the corrugations coupled to mechanistic articulation about the hinge lines. These are not independent kinematical modes; rather, they are prescriptive upon one another, resulting in a uniquely defined, low elastic stiffness in the same direction. The distribution and pattern of corrugations within the plane of the shell also determines any kinematical coupling, with the remaining modes being considerably stiffer. Understanding the relationship between the corrugation properties and the complete stiffness character of these shells is therefore imperative, so that their ability to carry loads and change shape safely is ensured. In this study, I begin by concentrating mainly on kinematical concepts, which aim

*kas14@cam.ac.uk

One contribution of 15 to a Theme Issue 'Geometry and mechanics of layered structures and materials'.

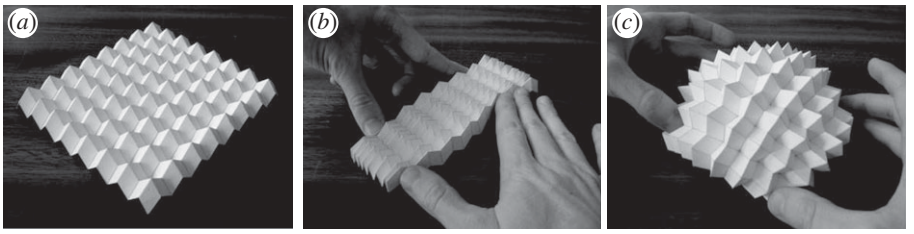

Figure 1. One type of compliant shell mechanism: a doubly and discretely corrugated 'egg-box' shell made from paper card. (*a*) A load-free, flat state. (*b*) The shell is manually compressed in a soft direction and extends in the orthogonal direction. (*c*) Out-of-plane bending to form a distinctive, doubly curved shape. These pictures are reproduced from Norman [1].

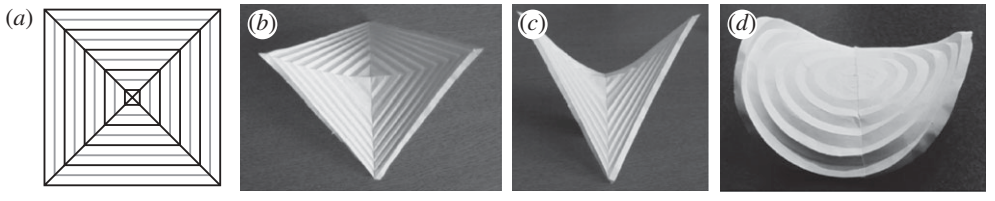

Figure 2. Hyperbolic paraboloids, or 'hypars', made by folding paper card. (*a*) A square-based hypar template: the black lines are folded in the opposite direction to the grey lines, to form corrugations. (*b*) The out-of-plane saddle shape that gives rise to the name of shell. (*c*) One of the parabolic saddle axes is more clearly visible. (*d*) A circle-based hypar with concentric corrugations, deforms in the same way by twisting out-of-plane.

to complement the general theme of layered structures in this Theme Issue, in the following way. Although the shells are essentially single-layered structures that can stretch and bend, I focus on capturing the *hierarchy* between the local, discrete nature of the shell and its overall shape. To this end, I define *meta-surfaces* that enforce compatibility requirements and afford a homogenized view of the global deformation. Thus, the 'layered' aspect underpins the analytical approach rather than being entirely based on physical properties.

I begin by distinguishing between shells that can be made by *developing*, or folding from, a flat sheet and those that are constructed in a non-developable manner, usually by joining flat strips along their edges. Strictly speaking, the former have no elastic stiffness in their soft directions because, by definition, the folding process itself is tantamount to an in-plane strain, which applies to every shape from the initial flat state of the sheet to the final state. The corrugated square-based hyperbolic paraboloid (or 'hypar') shown in figure 2 reveals something different. Even though it is formed in a developable manner, it becomes twisted overall into its namesake as the corrugations are made to close under in-plane compression. Locally, the corrugations also twist and resist further deformation, and the hypar now behaves as a compliant shell mechanism.

The hypar neatly indicates the hierarchical nature of the compatibility requirement between the corrugations and the overall shape, present in all compliant shell mechanisms. It also suggests, in a simplified way, how one may

begin to quantify these requirements. One may first neglect any local elastic deformation due to the developable assumption, provided the displacements are not too large. The intricate three-dimensionality of the shape can then be decoupled into the average, or *middle*, surface of the hypar and the effect of the corrugations opening or closing. The latter can be represented as an in-plane strain, which permits the shape of the middle surface to be found using one of two classical approaches. The first considers an extrinsic view, in which coordinate sets describe the shape of the middle surface in terms of an effective corrugation strain. The second approach uses intrinsic properties, where the overall shape is described by the Gaussian curvature and the angular defect of the sheet caused by the corrugation behaviour. These methods are described in §2 and are applied to both the square- and circular-based hypar; fair descriptions of behaviour are obtained despite the simplifying assumptions.

In §3, I present a curved corrugated shell, formed by joining curved strips of constant width along their adjacent edges. This shell is a true compliant mechanism in which each corrugation elastically deforms from the outset. There is also coupling between global modes, which is most simply demonstrated during unidirectional bending: when the shell is pulled apart across the corrugations, it becomes more tightly curved along them, and vice versa. The kinematical performance of the middle surface can be considered again in terms of an effective corrugation strain, which is formulated in terms of the invariant *geodesic* curvature of the original shell strips for a compact description. Because the shell deforms uniformly and inextensibly throughout, there is no spatial variation of shape in each corrugation: the strain energy stored in them can be found easily, and the large displacement stiffness of the shell follows without difficulty.

This shell also exhibits bidirectional bending into a cap or a saddle shape, and extremely so under larger displacements. This contradicts the general expectation of a developable shape such as a cone or a cylinder under asymptotic conditions, but it is an important result because it increases the range of possible geometrical transformations. The non-developable deformation is only apparent, as it is wrought by the corrugations opening and closing *non-uniformly* along their lengths. The sense of overall shape is better captured by thinking about each corrugation deforming between *bounding planes* rather than using the middle surface concept from before. The reason is subtle and will be explained, and it introduces another conceptual tool for tackling the kinematical hierarchy.

In §4, I consider doubly corrugated shells, returning to the egg-box in figure 1 and comparing it with the well-known developable Miura-ori shell. The egg-box is constructed differently, by interconnecting shaped strips, and thus it has embedded Gaussian curvature. During in-plane deformation, both exhibit high compliance but opposing Poisson effects: the Miura sheet expands or contracts in all directions and has a negative Poisson's ratio, whereas the egg-box has a positive Poisson's ratio. This is not unexpected if they are compared with ordinary materials, but they both show a remarkable reversal of Poisson effects during bending. I do not quantify this behaviour; rather, I describe a method for doing so, which is performed outside of this study. Finally, I present a summary and some open research questions in §5.

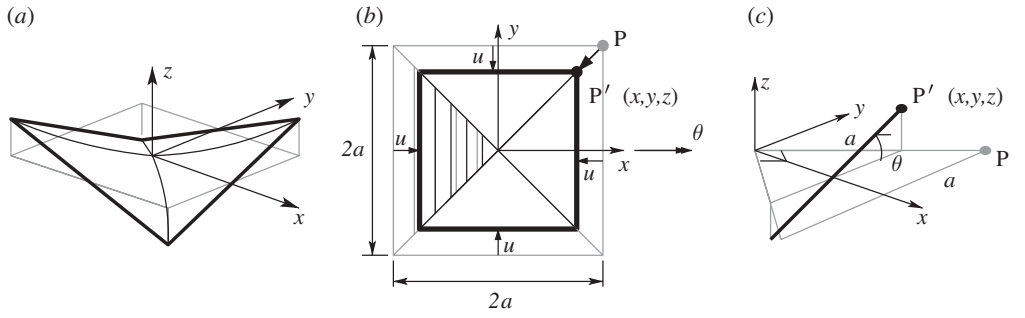

Figure 3. Extrinsic view of the hypar deformation. (*a*) The general and twisted out-of-plane shape, given by $z = \kappa_{xy} xy$. (*b*) A plan view of the symmetrical, in-plane displacement of the outer edges, u, where the corner point P moves along the projected diagonal line to P′. (*c*) The out-of-plane rotation of one of the outside edges, originally $x = a$, by angle θ.

2. Hyperbolic paraboloids

Creating hyperbolic paraboloids, or 'hypars', from pleated paper card was originally reported in Demaine *et al.* [3]. One template for a square hypar is given in figure 2*a* in which sets of hinge lines are scribed onto a flat sheet in four right-angle quadrants. Folding the hinge lines alternately to some non-zero angle forms the troughs and crests of the corrugations. As this angle increases, the hinge lines move closer together but rotate out of plane, and the original sheet adopts the characteristic saddle shape, as seen in figure 2*b*,*c*. A circular hypar with circumferential corrugations is shown in figure 2*d*, and it also twists out of plane as the corrugations are made to close.

(*a*) *Extrinsic view*

In figure 3*a*, the centre of a square hypar of side length $2a$ is located at the origin of an orthogonal set of axes, x, y, z. The alignment of the corrugations is chosen such that the out-of-plane shape of the middle surface is described by the twisted surface $z = \kappa_{xy} xy$, where κ_{xy} is the uniform twisting curvature: this is the simplest continuous description of shape. Accordingly, the saddle 'axes' are parabolae of opposite senses along the lines $y = \pm x$.

The closing of the corrugations is manifest extrinsically as a symmetrical in-plane contraction of the outside edges of the sheet. This is denoted as the displacement, u, in figure 3*b*, which gives rise to an effective corrugation strain, ϵ, measured relative to the original flat state as u/a. The outside edges are assumed to be axially rigid and they must also rotate by angle, θ, from the flat during contraction (figure 3*c*). Correspondingly, one of the corners of the sheet, P, moves to a new point, P′, with coordinates (x, y, z) such that

$$x = a(1-\epsilon), \quad y = a(1-\epsilon), \quad z = \kappa_{xy} xy = \kappa_{xy} a^2 (1-\epsilon)^2. \tag{2.1}$$

It is also evident from figure 3*c* that $\cos\theta = a(1-\epsilon)/a$ and $\sin\theta = z/a$. Substituting for z from (2.1), using the identity $\cos^2\theta + \sin^2\theta = 1$, and

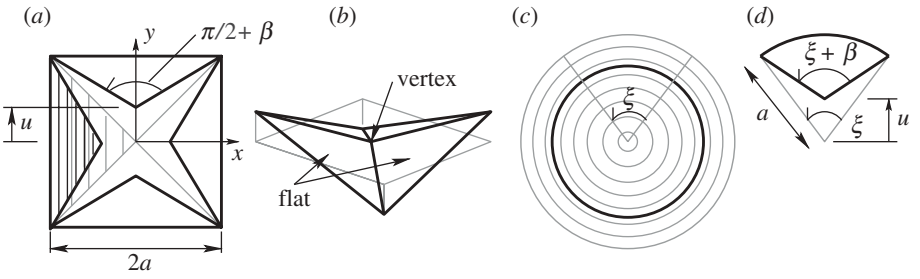

Figure 4. Intrinsic view of the hypar deformation. (*a*) A plan view of the deformed hypar, which has been laid flat after cutting along the intervening diagonals without changing the in-plane corrugation strain. The corresponding increase in the angle of each original quadrant is β, whose central vertex displaces by u. (*b*) The quadrants from (*a*) are now reconnected but without changing the corrugation strain. The quadrants remain as flat facets and meet at a vertex. (*c*) A general sector subtending angle ξ in a circular hypar. This sector in the deformed configuration is cut out and laid flat in (*d*) in the same manner as described in (*a*), where the sector angle increases to $\xi + \beta$.

rearranging, it can be verified that

$$\kappa_{xy}^2 = \frac{1}{a^2}\left[\frac{1-(1-\epsilon)^2}{(1-\epsilon)^4}\right]. \tag{2.2}$$

This expression correctly shows that the twisting becomes very large as ϵ tends to unity when the hypar contracts to virtually nothing; conversely, when $\epsilon \ll 1$, κ_{xy}^2 is approximately $2\epsilon/a^2$.

(*b*) *Intrinsic view*

Alternatively, consider the deformed hypar in figure 4*a*, which has been laid flat by cutting along both sets of diagonal lines but without changing the state of in-plane strain in each quadrant. If all corrugations are assumed to deform uniformly *and* identically, the quadrants remain triangular but are now obtuse. The increase beyond the right angle is denoted as β, and is formally known as the *angular excess* [4]. The corresponding in-plane displacement, u, can be measured outwards from the origin, and it is straightforward to calculate that

$$\tan\left(\frac{\pi}{4}+\frac{\beta}{2}\right) = \frac{1}{(1-\epsilon)} \quad \Rightarrow \quad \beta = 2\arctan\left(\frac{\epsilon}{2-\epsilon}\right), \tag{2.3}$$

in which the effective strain is again $\epsilon = u/a$: for small strains, $\beta \approx \epsilon$.

When the deformed quadrants are reconnected along their edges, the overall shape must twist out of plane (figure 4*b*). This shape appears to be a contracted hypar, but the middle surface of each quadrant remains flat within in its own plane and meets at a sharp vertex in the centre. This vertex is key, for the global shape can now be described in terms of a singular *Gaussian curvature* concentrated at the vertex, and measured according to the formal definition as [4]

$$g = \frac{\text{total angular defect}}{\text{associated area}}. \tag{2.4}$$

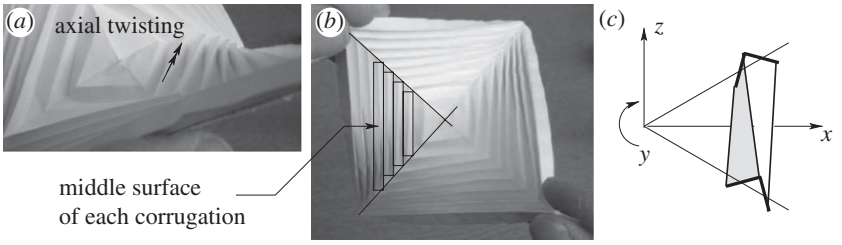

Figure 5. Local deformation of the corrugations in the square hypar. (*a*) Helical twisting of the hinge lines along their axes. (*b*) The net middle surface of each corrugation remains symmetrical and moves normal to the original hinge lines despite the helical twisting exhibited in (*a*) because the troughs and crests perform antisymmetrically. (*c*) A schematic of a single corrugation deforming out-of-plane under sizeable displacements. Along each quadrant edge, the ends of the corrugation are rotated in opposite senses, to maintain the continuity of shape with ends in adjacent quadrants, and this leads to the indicated twisting of hinge lines.

Strictly, g is the change in Gaussian curvature, the angular defect is the opposite of the angular excess and the vertex is encapsulated by the associated area of the original flat sheet: these properties are intrinsic, because they are specified without any coordinate system. This area ranges from zero to $4a^2$, and the total defect is -4β, with β given by equation (2.3).

(*c*) *Reconciliation of views*

Both of the previous approaches are valid but they present different global shapes: the intrinsic view predicts a concentrated Gaussian curvature, whereas the uniform twisting curvature of the extrinsic view conforms to a distributed and uniform Gaussian curvature, with $g = -\kappa_{xy}^2$ by definition. The former also assumes a uniform deformation at the level of each corrugation, in order to preserve the straight edges between the quadrants. However, the closing of the corrugations in the extrinsic view is implied without knowing the actual distribution of their fold angles: in other words, the *variation* of the effective in-plane strain afforded by them is not taken into account. This variation may be found by invoking the well-known compatibility relationship for surfaces [4]:

$$g = -\frac{\partial^2 \epsilon_x}{\partial y^2} - \frac{\partial^2 \epsilon_y}{\partial x^2} + \frac{\partial^2 \gamma_{xy}}{\partial x \partial y}. \tag{2.5}$$

The coordinate system is chosen so that the strain terms on the right-hand side can be correlated to the effective corrugation strains. For example, in the original quadrant, defined by $x > 0$ and bounded by the pair of lines $y = \pm x$, the hinge lines are directed along the y-axis, and the direct strain, ϵ_x, is the only viable strain in this region. Using equation (2.5), this strain must vary quadratically and, hence, non-uniformly, in the y-direction.

Closer examination of the deformed hypar in figure 5*a* reveals that the corrugations twist along their axes and that the hinge lines are no longer straight but modulate locally in a helical manner. This may suggest a non-uniform strain but the troughs and crests behave antisymmetrically with respect to each other, so that the middle surface associated with each corrugation, figure 5*b*, deforms

uniformly with respect to the original hinge line axis. The reason for the twisted hinge lines becomes apparent in figure 5*c*: the ends of each corrugation on the diagonal must rotate as the out-of-plane displacements increase.

The intrinsic approach offers a reasonable view of local behaviour but the predicted global shape is at odds with practice; the extrinsic formulation better describes the observed shape of hypar but it does not capture properly the expediting corrugation strains. The true behaviour is a mixture of both performances, and may be revealed in a more elaborate kinematical formulation: for example, in Demaine *et al.* [5], the twist along each corrugation can be achieved, or relieved, by additionally creasing each pleat for true developable behaviour. Another underlying reason is due to the inherent, discontinuous corrugation layout in the square hypar; in the case of the circular hypar with its continuous layout of corrugations, matters can be improved, and this is now performed as a final exercise.

(*d*) *Circular hypar*

Figure 4*c* indicates a sector of a circular hypar, which subtends an angle ξ in the original flat circle of radius a. An intrinsic viewpoint of the deformed hypar implies that this angle increases to $\xi + \beta$ while conserving the arc length of the outer edge and the straightness of the sector radial lines, as shown in figure 4*d*. This gives a nominal compressive radial strain, $\epsilon = u/a$, where u is the radial displacement of the centre, such that

$$a\xi = a(1-\epsilon)(\xi+\beta) \quad \Rightarrow \quad \beta = \frac{\epsilon\xi}{1-\epsilon}, \tag{2.6}$$

where β is, again, the angular excess. The Gaussian curvature of the entire hypar considers $2\pi/\xi$ sectors and, using equation (2.4),

$$g = \frac{-\beta(2\pi/\xi)}{A} = -\frac{1}{A}\frac{2\pi\epsilon}{1-\epsilon}, \tag{2.7}$$

where A is the associated area. Note that the result is independent of the original sector angle, and the formulation may therefore be stated in elemental terms, although the Gaussian curvature is still concentrated at the centre of the shell. Consequently, the out-of-plane shape is continuous; if one thinks of a cone being formed by creating an angular defect in a circular sheet, then the intrinsic view of the circular hypar must have the opposite shape to the cone.

As far as an extrinsic view is concerned, it is convenient to refer to an axisymmetrical coordinate system, because the effective corrugation strain acts in the radial direction only and there is a hoop-wise uniformity in shape as well as inextensibility in this direction. The Gaussian curvature is assumed to be uniform throughout the shell, equal to some negative value of g. The variation in effective strain can be found from equation (2.5), by writing it in terms of a radial coordinate, r, and associated tensile strain, ϵ_r, and integrating twice, to reveal

$$g = \frac{1}{r}\frac{\partial\epsilon_r}{\partial r} \quad \Rightarrow \quad \epsilon_r = -\epsilon = \frac{gr^2}{2}. \tag{2.8}$$

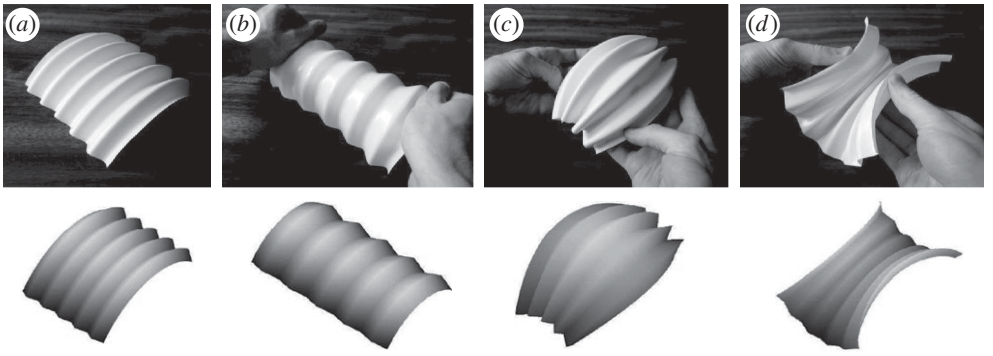

Figure 6. A curved corrugated shell: the top row is reproduced from Norman & Seffen [6] and the bottom row denotes predictions of shape following the solution of equation (3.7). The physical shell is not made from paper card but from plastic. (*a*) The initial, stress-free shape. (*b*) Unidirectional bending, where a transverse extension produces a more tightly coiled structure. Bidirectional bending follows in (*c*) and (*d*) with positive and negative Gaussian curvature overall, respectively. The simulated shapes have $w = 10\,\mathrm{mm}$ and $\kappa_g = 1/100\,\mathrm{mm}^{-1}$, and values of θ_0 and α, defined in figure 8*c*, as: (*a*) $50°, 0°$; (*b*) $70°, 0°$; (*c*) $60°, +8°$; (*d*) $60°, -8°$.

The final strain expression is the simplest possible, assuming that there is no strain at the hypar centre. Radial compression arises naturally and becomes larger towards the periphery, as observed in practice, and confirmed in Demaine *et al.* [5].

In closing, these two views deal with different global shapes, but, unlike the square hypar, they are both continuous in nature even though they differ in terms of the order of distribution of Gaussian curvature. The extrinsic view, again, must assume that the Gaussian curvature is distributed throughout the shell, and this is a reasonable interpretation from the practical model. The intrinsic view still works with a singular Gaussian curvature but now the shape is continuous everywhere else; essentially, the principal curvature in the radial direction is zero but not in the hoop-wise direction, and this ensures that the Gaussian curvature outside of the vertex can be zero.

3. Curved corrugated shells

Figure 6*a* shows a corrugated shell initially curved along the corrugation axes and forming an open cylindrical shape. When the shell is pulled apart, it becomes more tightly coiled, and vice versa (figure 6*b*). But unlike the previous hypars, the shell can acquire positive or negative Gaussian curvature: depending on the direction of transverse bending, it can become doubly curved with curvatures in the same sense (figure 6*c*), or adopt the familiar saddle shape with curvatures in opposite senses (figure 6*d*).

The kinematics of the simpler case of 'unidirectional' bending can be treated like the hypars, by assessing the performance of the middle surface of the shell. The shell is constructed by joining together curved strips, similar to the template in figure 7*a*, along their edges to form a compact, stress-free stack of strips. When the stack is opened, the global curvature increases as each strip bends into a tighter conical section.

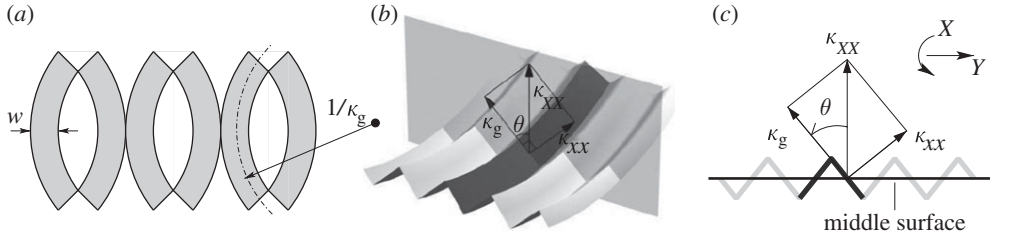

Figure 7. (*a*) A curved corrugated shell is made by taking identical curved strips of constant width, w, centreline curvature, κ_g, and interconnecting them on adjacent edges as shown. (*b*) The resulting shape of the shell is described by three curvatures, located on the centreline of a given corrugation (in black): κ_{XX}, the overall cylindrical curvature of the middle surface; κ_g, known as the geodesic curvature; and κ_{xx}, the local out-of-plane shell curvature of the strip. (*c*) Formal cross-sectional view of the curvatures and their directions, related by the fold angle, θ. The middle surface is located halfway between troughs and crests, and X and Y are global coordinates.

This curvature is formally designated as the curvature of the middle surface, and is denoted as κ_{XX}, where X is a global coordinate running along the corrugation axes (figure 7*b*). Importantly, κ_{XX} is composed of two orthogonal components of curvature, related by the corrugation fold angle, θ (figure 7*b*,*c*). The first component is the *geodesic* curvature, κ_g, of the centreline of the original flat strips: this is an *invariant* quantity that is parallel to the strip width. The second is the local shell curvature, which acts normal to the strips and is denoted by κ_{xx}, where the local coordinate, x, is parallel to X. In the same cross-sectional view, the corrugations are assumed to remain straight and untwisted, so there is no other shell deformation, and the Y-direction is transversal and global. The width of the strips, w, is also assumed to be much thicker than the local thickness of the shell itself.

Let ϵ_Y denote the effective in-plane corrugation strain of the middle surface, measured relative to the flattened corrugated state. Simple geometry gives

$$\epsilon_Y = 1 - \sin\theta, \quad \kappa_{XX} = \frac{\kappa_g}{\cos\theta}, \tag{3.1}$$

which can be combined into a single expression using $\cos^2\theta + \sin^2\theta = 1$, then explicitly written in terms of the global cylindrical curvature as

$$\kappa_{XX}^2 = \frac{\kappa_g^2}{[1-(1-\epsilon_Y)^2]}. \tag{3.2}$$

When $\theta = 0$, the corrugations are completely folded, $\epsilon_Y = 1$, and κ_{XX} is correctly equal to κ_g. As the corrugations flatten, ϵ_Y tends to zero and κ_{XX} becomes very large: the shell becomes very tightly coiled and much stiffer in practice. If $1/\kappa_g \gg w$, the curvature change everywhere in each strip is approximately equal to κ_{xx}, and an approximate expression for the strain energy stored in bending in the shell is given by the shell area multiplied by the strain energy density, which is equation (2.33) of Calladine [4]: $(D/2)[(\kappa_{xx}+\kappa_{yy})^2 - 2(1-\nu)(\kappa_{xx}\kappa_{yy} - \kappa_{xy}^2)]$; the flexural rigidity of the shell is D and the Poisson's ratio is ν. Here, κ_{yy} and κ_{xy} are both zero and, from figure 7*c*, $\kappa_{xx} = \kappa_g \tan\theta$. Thus, the total strain energy

increases rapidly as the corrugations open owing to the presence of the $\tan^2\theta$ term, and the corresponding transverse stiffness may be formally ascribed by differentiating the strain energy expression twice with respect to θ.

The kinematical relationships in equations (3.1) and (3.2) were first determined by Norman *et al.* [7], who also proposed a bidirectional bending model using the middle surface approach. They assume reasonably that the fold angle, θ, varies along the corrugations in the X-direction to yield double curving of the middle surface. To make the analysis tractable, they also assume that $\theta = \theta(X)$ only, which dictates that the troughs and crests are identically open along a given Y-latitude. It is possible to make the shell bend this way by carefully manipulating it by hand, but it seems an unnatural mode. The more natural shape in either figure 6*c* or *d* is simply held, and closer inspection suggests that, on a given latitude, the fold angles are the same for the troughs, and for the crests, but different from each other. It is not obvious how the middle surface approach can be adapted for this, for it subsumes the discrete corrugation nature when a discrete formulation is needed.

Instead, consider a single corrugation in the shell, which has been extracted in isolation, but which deforms identically because the boundary conditions with adjacent corrugations are properly maintained: all of the other corrugations behave exactly the same. Figure 8*a* shows a corrugation with an arbitrary uniform fold angle throughout, corresponding to the case of unidirectional bending. Each hinge line lies in a plane, and all planes are vertical: only the outer planes are highlighted, and they move apart as the corrugation fold angle changes; in this figure, the outer hinge lines are troughs. During bidirectional bending, the outer planes tilt towards each other and form a wedge space and (shown in figure 8*b*) the outer hinge lines continue to touch the planes everywhere along their lengths. Note also that the fold angle at the troughs is larger than that at the crests, as observed.

Figure 8*c* indicates the origin, O, of the XY coordinate system located at the top of the corrugation. There is a vertical symmetry plane passing through the crest line, and various semi-angles are specified: the wedge space semi-angle is α; the corrugation fold angle at the crest is θ, and equal to θ_0 at O. The variation of θ with arc length, s, ensures that the distance from the crest line to each tilted plane is the strip width, w. Extra schematic detail is furnished in figure 9*a*. The global radius of curvature of the crest is denoted by ρ, which emanates from a point, C, beneath the corrugation. Recall that the original geodesic curvature of the strip centreline is κ_g, so that

$$\rho = \left(\frac{1}{\kappa_g} + \frac{w}{2}\right)\cos\theta. \tag{3.3}$$

The vertical inclination of ρ is defined to be η, and an elemental change in arc length, δs, is equal to $\rho\delta\eta$.

Three additional points in line with ρ are highlighted: R, on the wedge vertex line; Q, at the corrugation edge on the inclined plane; and P on the crest. The true cross-sectional view in a tangential direction to P also shows these points, the fold angle, θ, and the component of the wedge semi-angle, α'. The relationship to α is found easily as

$$\tan\alpha' = \cos\eta\tan\alpha, \tag{3.4}$$

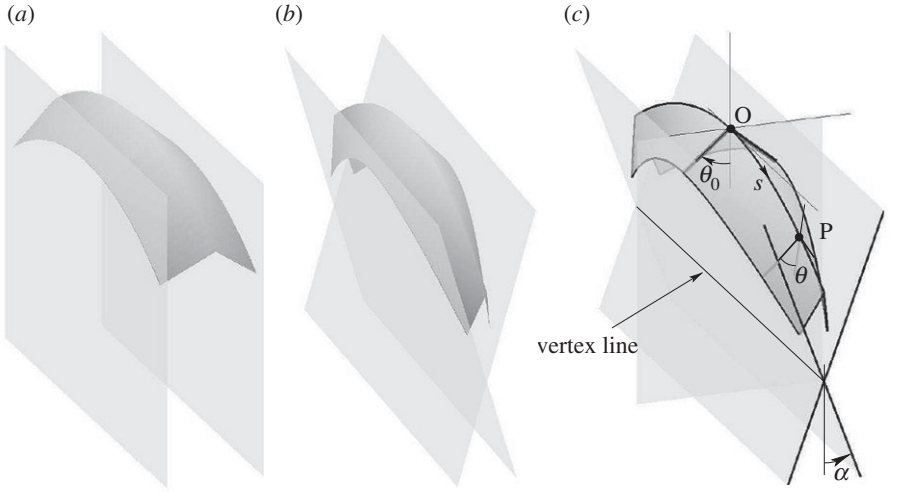

Figure 8. Deformation of a single corrugation within a curved corrugated shell. (*a*) The corrugation has a uniform fold angle everywhere and the outer hinge lines lie in vertical, parallel planes. (*b*) Transverse bending of the entire shell causes the outer planes in (*a*) to tilt: this forms a wedge space and the outer hinges maintain contact with these planes, in order to preserve the local distortion of the corrugation within the shell. (*c*) As (*b*), the degree of transverse bending is measured by the wedge space semi-angle, α, the fold angle varies from θ_0 at the origin, O, to θ at a general point, P, at an arc length, s, from O. The origin is located at the top of the corrugation.

and the length of PR is given by $w\cos\theta + w\sin\theta/\tan\alpha'$. The horizontal projection of CR is equal to $(\rho - \mathrm{PR})\cos\eta$, and this is conserved when P advances by δs to P′ if the wedge space is assumed to be uniform, with corresponding elemental increases in θ and η, i.e.

$$(\rho - \mathrm{PR})\cos\eta = (\rho - \mathrm{P'R'})\cos(\eta + \delta\eta). \tag{3.5}$$

Expanding and simplifying, one has

$$\left[\rho - w\cos\theta - \frac{w\sin\theta}{\tan\alpha\cos\eta}\right]\cos\eta$$
$$= \left[\rho - w\cos(\theta+\delta\theta) - \frac{w\sin(\theta+\delta\theta)}{\tan\alpha\cos(\eta+\delta\eta)}\right]\cos(\eta+\delta\eta)$$
$$\Rightarrow \quad \rho\sin\eta\,\delta\eta + \frac{w\cos\theta\,\delta\theta}{\tan\alpha} - w\cos\theta\sin\eta\,\delta\eta - w\sin\theta\cos\eta\,\delta\theta = 0. \tag{3.6}$$

Rearranging (3.6), observing the limit as all elemental quantities tend to zero, and substituting for ρ from equation (3.3) and $\phi = (1/\kappa_g - w/2)/w$, finally reveals the governing differential equation for the evolution of the fold angle as

$$\frac{\mathrm{d}\theta}{\mathrm{d}\eta} = \frac{\phi\tan\alpha\sin\eta}{\tan\alpha\tan\theta\cos\eta - 1}. \tag{3.7}$$

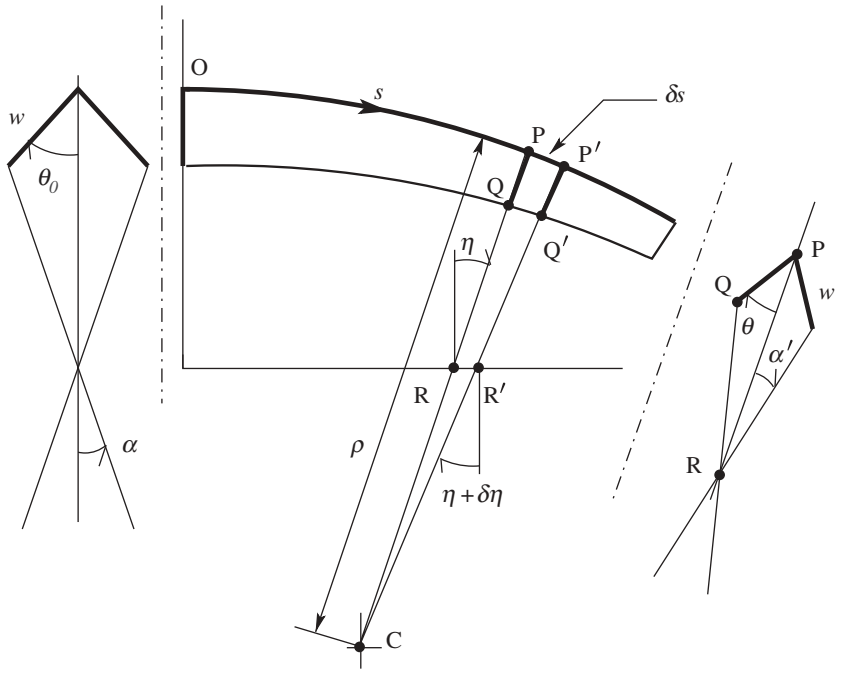

Figure 9. Schematic elevation of the forward half of the corrugation from figure 8*c*. The radius of curvature of the crest line is ρ at P, which is inclined at η to the vertical, and emanates from a point C. Point R lies on the vertex line (figure 8*c*) and Q is on the edge of the corrugation, so that they form a true view, which shows the fold angle, θ, and the component of the wedge-space semi-angle, α'. The true view at the origin shows the true wedge angle, α. All quantities are defined for transverse bending with respect to positive Gaussian curvature.

This can be solved numerically for specified values of α, ϕ and θ_0. Predictions of shape are informally compared with models in figure 6, where the shape of a single corrugation is computed and then reflected about successive edge planes to form the complete shell. As can be seen, there is a favourable correlation, encouragingly so when the displacements are clearly large.

Finally, note that equation (3.7) can be simplified when α is small by setting the denominator equal to unity. It may be integrated directly to give

$$\frac{\mathrm{d}\theta}{\mathrm{d}\eta} \approx \phi \tan\alpha \sin\eta \quad \Rightarrow \quad \theta = \theta_0 \mp \phi \tan\alpha(1-\cos\eta). \tag{3.8}$$

The minus sign applies when the shell is bent with positive Gaussian curvature so that, as expected, the fold angle decreases outwardly from the corrugation centre, and vice versa.

4. Doubly corrugated shells

The previous shells are singly corrugated structures with non-intersecting hinge lines. The shell in figure 10 is made by interconnecting the pattern of undulating flat strips in figure 10*a* along their adjacent edges [1]. This produces a globally flat

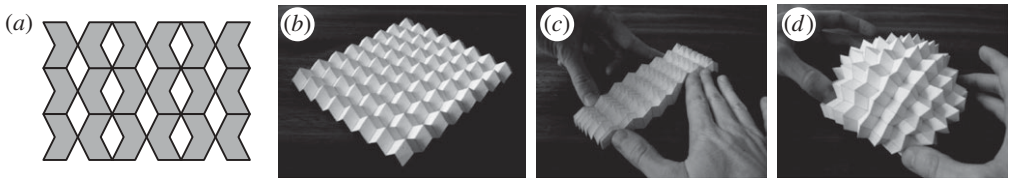

Figure 10. More detail on the egg-box shell from figure 1. (*a*) The shell is constructed from identical strips in which adjacent edges are connected to form one set of hinge lines, while another set is formed by folding across the strips along the indicated black lines. (*b*) One globally flat state, which is compressed in-plane in (*c*): although it is difficult to see, the shell expands in the direction normal to compression, giving rise to a positive effective Poisson's ratio. (*d*) Out-of-plane bending of the shell produces synclastic, or same-sense, curvatures, which suggests a negative Poisson's ratio.

egg-box shell, figure 10*b*, with orthogonal sets of overlapping hinge lines, resulting in a doubly corrugated form. The shell is compliant in directions parallel to the hinge lines, but these modes are coupled: when it is compressed or stretched in-plane, accordingly, it expands or contracts in the other direction (figure 10*c*), and vice versa. The effective performance asserts a positive Poisson's ratio—as in most engineering materials. The shell also resists any shear deformation of the hinge lines and is stiff in this mode, and stiffening due to interference of the hinge lines is not considered.

Unlike singly corrugated shells, movement along one of the compliant directions is relieved by the second without need of out-of-plane distortions. Bending alone, however, is remarkable, as noted in §1. Figure 10*d* shows that there is double curving in the same sense and the global shape resembles a spherical cap. These *synclastic* curvatures are associated with materials in which the Poisson's ratio is negative, and this clearly conflicts with the in-plane performance.

The Miura-ori shell in figure 11 also has intersecting hinge lines but it differs physically from the egg-box in two ways. It is developable and the hinge lines are crooked; and a typical folding pattern is indicated. Its corresponding in-plane behaviour is well known and has been used to explain, for example, folding mechanisms in leaves [8]: its effective Poisson's ratio is negative, and the sheet expands in all directions when pulled transversely, and vice versa. This is quite different from the egg-box; but like the egg-box, the effective Poisson's ratio in bending is reversed, and the Miura-ori shell deforms with anticlastic curvatures when it is bent transversely.

Separately, both shells have paradoxical in-plane and out-of-plane performances, and together they behave in a contradictory fashion to one another. Their effective properties are therefore novel and they also demonstrate that a globally flat sheet can acquire Gaussian curvature overall. Thus far, only the in-plane kinematics of the Miura-ori shell have been extensively studied, usually by means of a unit cell approach, owing to the repetitive pattern formed by the hinge lines when viewed in plan; the key to its negative Poisson's ratio is the *re-entrant* profile of this unit cell [9].

Curving of the Miura-ori shell is less well understood; in particular, how to formulate accurate assumptions about the deformation of the shell facets, for it is clear from handling the sheet that the facets do deform locally, and overall

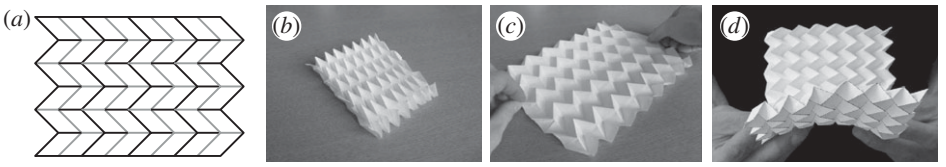

Figure 11. A doubly corrugated shell using the Miura-ori folding pattern. (*a*) This pattern comprises two sets of differently coloured hinge lines, which are folded in opposite senses; for example, the grey lines form valleys and black lines form ridges. (*b*) One initial flat state, which expands in all directions in (*c*) upon unidirectional in-plane extension. (*d*) Bending out-of-plane results in anticlastic curvatures. The effective Poisson's ratios in (*c*) and (*d*) are negative and positive, respectively, in opposition to the previous egg-box shell.

it behaves as a compliant shell mechanism. One recent numerical scheme uses a folded plate model [10] in which the facets are subdivided into rigid triangular plates capable of rotating relative to each other, in order to simulate local bending with a specified stiffness. Early results are promising and the final study will be published elsewhere [11]. The folded plate model has also been used to devise a global stiffness matrix for the egg-box, which is then used in a modal vibration analysis to reveal the natural mode shapes [1]. This approach confirms that same-sense double curving is indeed a low-stiffness mode and is a preferential deformed shape. It is, however, an holistic approach, it requires an elaborate discretization scheme, and it does not inform explicitly on the hierarchical nature of deformation.

I propose that the latter can be ascribed to unit cells deforming identically within constraining planes obviated by the global deformation of the sheet: this is similar to the case of the corrugated shell in §2, except that there are more than two bounding planes. The particular unit cell is revealed in figure 12*a* by first highlighting the salient vertices and then choosing the simplest symmetrical cell without cutting any of the facets. The cell comprises four facets, figure 12*b*, and the internal hinge lines are, respectively, inclined at angles θ_1 and θ_2 to the horizontal. The periphery of the cell is the outer hinge lines, and these always touch the bounding planes and have relative inclinations θ_3 and θ_4. All angles are semi-angles because the modes considered here are globally symmetrical. They are not independent angles but are related under the constraints of the imposed deformation. For example, figure 12*c* shows compression of the unit cell in one direction with orthogonal expansion. This is accomplished by the bounding planes moving but remaining vertical, and by the hinge lines rotating: θ_1 and θ_3 increase, and θ_2 and θ_4 must decrease. Moreover, $\theta_1 = -\theta_2$, if the rotations are assumed to be small, and the angular defect of the vertex remains unchanged: there is no planar stretching or compression of each facet, whose geometry may therefore be assumed to remain fixed, which leads to a fairly straightforward determination of an effective positive Poisson's ratio. Figure 12*d* instead displays the unit cell deforming when there is spherical curving overall. It is clear in this case that, as the planes tilt symmetrically towards each other, θ_1 and θ_2 must increase, and θ_3 and θ_4 decrease. Correspondingly, the angular defect of the vertex also changes, and this invokes stretching or compression of the facet when its edges are constrained to lie within the bounding planes. In response, each facet appears

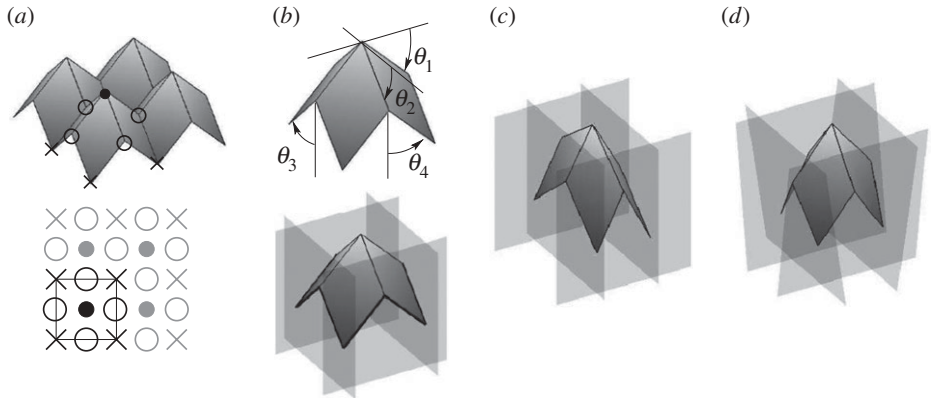

Figure 12. Deformation of a unit cell from the egg-box shell. (*a*) Distinguishing between the vertices allows identification of a unit cell with four facets. (*b*) Two views of the unit cell taken within a globally flat sheet. Top: inclination angles, θ_1 to θ_4, which apply to each pair of hinge lines; bottom: the unit cell periphery of the emboldened hinge lines always lies within the bounding planes, which themselves conform to the global deformation of the sheet. (*c*) Pure in-plane deformation of the cell. Compared with (*b*), θ_1 and θ_3 increase, and θ_2 and θ_4 decrease. The bounding planes are vertical and their displacements show the effective Poisson's ratio as being positive. (*d*) Unit cell deformation under global double curving in the same sense. Compared with (*b*), θ_1 and θ_2 increase, and θ_3 and θ_4 decrease. The bounding planes tilt towards each other to reveal a negative Poisson's ratio.

to bend about either of its symmetry axes on closer inspection. As a corollary, it is suggested that developable behaviour arises if extra hinge lines are introduced into each facet along either axis, to relieve this bending in a manner similar to additionally creasing the pleats in the square hypar [5]: for a more detailed exposition, the reader is referred to Schenk's thesis [11]. Nonetheless, a negative Poisson's ratio is plausible, and feasible, under double curving, but the in-plane behaviour of each facet cannot be ignored. Finally, it is worth remarking that the tilting angles between successive unit cells cannot be the same throughout the egg-box; rather, they must vary in both directions, because otherwise the cells will not fit together to reveal a uniformly curved surface.

5. Summary

Compliant shell mechanisms are discretely corrugated structures, capable of undergoing large, reversible displacements. As well as being soft in certain directions and stiff in others, their shape-changing potential garners interest here compared with ordinary smooth shells: they are developable, they can furnish apparent changes in Gaussian curvature and they can offer a breadth of coupled modes with different Poisson's ratios. The changes in shape are dictated by the corrugation layout and by the nonlinear interaction of local elastic deformation and rigid-body articulation afforded by the corrugations themselves. Thus, there is a clear kinematical hierarchy, and I have attempted to highlight this through the behaviour of specific and fairly well-known corrugated shells from disparate studies.

Our understanding has been guided by two views. First, consider the entire shape of the shell through its middle surface alone, which is taken to be smooth and continuous. The corrugations are discounted physically but their effect is incorporated as compatible local strains that inform the shape of the middle surface. Alternatively, take a local view at the level of the corrugation, in isolation from the rest of the shell. This isolated portion, or unit cell, deforms by adhering to the correct boundary conditions on its periphery: these are symmetrical by definition and correctly reflect the overall shape of the shell. For pure in-plane behaviour, this is relatively straightforward to execute and, typically, the corresponding effective properties can be used to describe the out-of-plane bending properties. However, this is not feasible if these two responsive modes behave in a contradictory fashion—cf. the conflicting Poisson's ratios in the doubly corrugated shells. This has been resolved by proposing that the unit cell is bounded by planes that can move apart or tilt in accordance with the overall deformation: the unit cell locally deforms and articulates as it moves within the volumetric space created by the planes; and, to the author's knowledge, this is a novel approach.

There are many avenues of further research. The shells here are simply made using regular template patterns, and it is not difficult to envisage other, possibly irregular or non-uniform, patterns. These may help to answer what are clearly open questions about the influence of the corrugation topology upon the character of the compliant modes. For example, here I have shown that there is direct coupling between in-plane and out-of-plane modes when the shells are singly corrugated, but in doubly corrugated cases, the coupling effect is more subtle. It is also important to consider how to make practical shells using traditional materials, such as metals, which oblige because of their ductility and their relative ease of forming. Finally, their complete structural behaviour must be understood: the ability to change shape effectively has to be balanced by the structure being stiff in other modes. These and other questions are currently being answered by the Advanced Structures Group at Cambridge.

K.A.S. gratefully acknowledges the invitation from the editor to write this paper for this Theme Issue. Mark Schenk and Alex Norman are thanked for their photographs of doubly corrugated shells, and the former is thanked for many stimulating discussions on this paper.

References

1 Norman, A. D. 2009 Multistable and morphing corrugated shell structures. PhD thesis, University of Cambridge, Cambridge, UK.

2 Weiss, P. 2003 Wings of change: shape-shifting aircraft may ply future skyways. *Sci. News* **164**, 359. (doi:10.2307/4018925).

3 Demaine, E. D., Demaine, M. L. & Lubiw, A. 1999 Polyhedral sculptures with hyperbolic paraboloids. In *Proc. 2nd Annual Conf. of BRIDGES: Mathematical Connections in Art, Music and Science, Southwestern College, Winfield, KS, 30 July–1 August 1999* (ed. R. Sarhangi), pp. 91–100. See http://erikdemaine.org/papers/BRIDGES99/paper.pdf.

4 Calladine, C. R. 1983 *Theory of shell structures*. Cambridge, UK: Cambridge University Press.

5 Demaine, E. D., Demaine, M. L., Hart, V., Price, G. N. & Tachi, T. 2011. (Non)existence of pleated folds: how paper folds between creases. *Graphs Comb.* **27**, 377–397. (doi:1007/s00373-011-1025-2)

6 Norman, A. D., Seffen, K. A. & Guest, S. D. 2008 Multistable corrugated shells. *Proc. R. Soc. A*, **464**, 1653–1672. (doi:10.1098/rspa.2007.0216)

7 Norman, A. D., Seffen, K. A. & Guest, S. D. 2009 Morphing of curved corrugated shells. *Int. J. Solids Struct.* **46**, 1624–1633. (doi:10.1016/j.ijsolstr.2008.12.009)
8 De Focatiis, D. S. A. & Guest, S. D. 2002 Deployable membranes designed from folding tree leaves. *Phil. Trans. R. Soc. Lond. A* **360**, 227–238. (doi:10.1098/rsta.2001.0928)
9 Mahadevan, L. & Rica, S. 2005 Self-organised origami. *Science* **307**, 1740. (doi:10.1126/science.1105169)
10 Schenk, M. 2008 Textured shell structures. First-year PhD report, University of Cambridge, Cambridge, UK.
11 Schenk, M. 2012 Textured shell structures. PhD thesis, University of Cambridge, Cambridge, UK.